Synthesis, Structure, and Electronic Properties of a Mixed-Valent Dodecairon Oxo Complex, a Model for the Biomineralization of Ferritin

Kingsley L. Taft,[1a] Georgia C. Papaefthymiou,[1b] and Stephen J. Lippard*,[1a]

Department of Chemistry and Francis Bitter National Magnet Laboratory, Massachusetts Institute of Technology, Cambridge, Massachusetts 02139

Received September 20, 1993®

The mixed-valent polyiron oxo complex $[Fe^{III}_4Fe^{II}_8(O)_2(OMe)_{18}(OAc)_6(MeOH)_{4.67}]$ (**1**) was prepared through the controlled oxidation of a methanol solution of ferrous acetate and lithium methoxide. The structure of **1**, revealed in a single-crystal X-ray diffraction experiment, consists of a face-centered cubic array of oxygen atoms with iron(II) and iron(III) ions in the octahedral interstices. Two μ_6-oxo ligands, to which ten of the twelve iron atoms are coordinated, form the core of the structure. The iron atoms have distorted octahedral coordination geometries with oxo, methoxide, methanol, and acetate ligands. From an analysis of the Fe–O bond lengths and from charge considerations, four of the twelve iron atoms were assigned as ferric ions. Crystals of **1** are air-sensitive and lose coordinated methanol when removed from the reaction solution. The mixed-valent nature of **1** was further characterized by electronic spectroscopy. There is a broad feature at 694 nm with shoulders at 900 and 1250 nm attributable to iron(II) ligand field and intervalence charge transfer transitions. The iron atoms of **1** exhibit overall antiferromagnetic exchange coupling, with χT decreasing from 40.3 emu mol^{-1} K at 300 K to 7.04 emu mol^{-1} K at 2.5 K. The calculated spin-only χT value for four iron(III) ions with $g = 2.0$ and eight iron(II) ions with $g = 2.2$ is 46.5 emu mol^{-1} K. No saturation was observed in a high-field magnetization study of **1** at 1.4 K, the maximum value attained being 18.2 μ_B at 20.0 T. Mössbauer spectral studies of **1** at 20 K revealed three distinguishable quadrupolar doublets, one with spectral parameters characteristic of iron(III) ($\delta = 0.47$ and $\Delta E_Q = 0.74$ mm s^{-1}) and two quadrupolar resonances arising from iron(II) ions ($\delta = 1.28$ and 1.29 and $\Delta E_Q = 2.02$ and 3.29 mm s^{-1}, respectively). The relative absorption areas for the three spectral features were consistent with the foregoing assignment of oxidation states. No valence delocalization was observed for **1** up to 250 K. Below 20 K, intermediate relaxation phenomena were evident for all three quadrupole doublets. The temperature dependence of the Mössbauer spectra was consistent with superparamagnetism, such as that observed for the mineral core of the iron storage protein ferritin. The exact source of the slow spin relaxation in **1** has proved difficult to identify unequivocally, however. The method used to prepare **1**, oxidation of iron(II), and its structure, a lattice array of oxygen and iron atoms, compare favorably with the biomineralization process and structure of the mineral core in ferritin, respectively. Crystallographic data for **1** at 185 K are as follows: $P\bar{1}$, $a = 11.868(2)$ Å, $b = 13.309(2)$ Å, $c = 10.437(2)$ Å, $\alpha = 100.96(2)°$, $\beta = 95.30(2)°$, $\gamma = 80.07(1)°$, $V = 1591.2(5)$ Å^3, $Z = 1$, $M_r = 1764.67$, $\rho_{calc} = 1.841$ g cm^{-3}. For 4709 unique observed reflections collected at 185 K with $F^2 > 3\sigma(F^2)$, $R = 0.054$ and $R_w = 0.071$.

Introduction

The chemistry of iron with oxygen donor ligands is dominated by oxidation and hydrolytic processes which produce insoluble iron(II) and iron(III) oxides.[2] Numerous chemical and mineralogical examples are known.[3,4] The biological processing of iron requires the careful control of these two reactions.[5] Uncontrolled oxidation of iron(II) can generate toxic hydroxyl radicals, and hydrolysis deposits iron(III) oxides which are biologically inaccessible and potentially harmful.[2,5] The iron storage protein ferritin (Ft) provides a safe, bioavailable harbor for iron in living organisms.[6] Ft solubilizes up to 4500 iron(III) atoms in its iron–oxo–hydroxo mineral core by surrounding it with a protein coat.

In vertebrates, the Ft apoprotein consists of 24 subunits designated L or H. The inorganic core, which is 70–80 Å in diameter, is encapsulated by the polypeptide sheath, which can have a variable ratio of the two different subunits. X-ray structures of several forms of the apoprotein have been completed.[6,7] In contrast, the detailed structure of the inorganic core of Ft remains ill-defined. Numerous studies indicate that iron exists in the ferric state and has an octahedral geometry with exclusively oxygen donor atoms. A relationship between the mineral ferrihydrite, which has the composition $5Fe_2O_3 \cdot 9H_2O$, and the Ft core has been established, on the basis of their similar powder diffraction patterns.[6,8] Depending upon the source of the Ft protein and the reconstitution conditions, phosphate can also be incorporated into the core. The structural consequences of increasing phosphate concentration are not clear although, as the percentage of phosphate increases, long-range order in the core is diminished. To provide a better understanding of the structural and physical properties of iron–oxo–hydroxo species in Ft

* Abstract published in *Advance ACS Abstracts*, March 1, 1994.

(1) (a) Department of Chemistry. (b) Francis Bitter National Magnet Laboratory.

(2) (a) Flynn, C. M. *J. Chem. Rev.* **1984**, *84*, 31. (b) Schneider, W. *Comments Inorg. Chem.* **1984**, *3*, 205. (c) Schneider, W. *Chimia* **1988**, *42*, 9.

(3) (a) Lippard, S. J. *Angew. Chem., Int. Ed. Engl.* **1988**, *27*, 344. (b) Hagen, K. S. *Angew. Chem., Int. Ed. Engl.* **1992**, *31*, 1010.

(4) (a) Murray, J. W. In *Marine Minerals*; Burns, R. G., Ed.; Mineralogical Society of America: Washington, DC, 1979; pp 47–98. (b) Murad, E.; Johnston, J. H. In *Mössbauer Spectroscopy Applied to Inorganic Chemistry*; Long, G. J., Ed.; Plenum: New York, 1987; Vol. 2; pp 507–582.

(5) Crichton, R. R. *Inorganic Biochemistry of Iron Metabolism*; Horwood: New York, 1991.

(6) For reviews of Ft chemistry, see: (a) Ford, G. C.; Harrison, P. M.; Rice, D. W.; Smith, J. M. A.; Treffry, A.; White, J. L.; Yariv, J. *Philos. Trans. R. Soc. London* **1984**, *B304*, 551. (b) *Biomineralization: Chemical and Biochemical Perspectives*; Mann, S., Webb, J., Williams, R. J. P., Eds.; VCH: New York, 1989; pp 257–344. (c) Artymiuk, P. J.; Bauminger, E. R.; Harrison, P. M.; Lawson, D. M.; Nowik, I.; Treffry, A.; Yewdall, S. J. In *Iron Biominerals*; Frankel, R. B., Blakemore, R. P., Eds.; Plenum: New York, 1991; pp 269–294.

(7) Lawson, D. M.; Artymiuk, P. J.; Yewdall, S. J.; Smith, J. M. A.; Livingstone, J. C.; Treffry, A.; Luzzago, A.; Levi, S.; Arosio, P.; Cesareni, G.; Thomas, C. D.; Shaw, W. V.; Harrison, P. M. *Nature* **1991**, *349*, 541.

(8) Towe, K. M.; Bradley, W. F. *J. Colloid Interface Sci.* **1967**, *24*, 384.

0020-1669/94/1333-1510$04.50/0

containing partially or fully loaded cores, several discrete, high-nuclearity iron oxo complexes have been prepared and structurally characterized.[3,9-14] These molecules were usually isolated by hydrolysis of iron(III) reagents in the presence of organic ligands that mitigate the aggregation process. It is believed that the mineral core of Ft is generated by oxidation of iron(II) followed by hydrolysis in vivo, however, and it is almost always generated in this manner in vitro.

Following a similar synthetic strategy, we have prepared and characterized a novel mixed-valent polynuclear iron complex having the molecular formula $[Fe^{III}_4Fe^{II}_8(O)_2(OMe)_{18}(OAc)_6(MeOH)_{4.67}]$ (**1**). Deep green crystals of **1** were isolated upon the air oxidation of a solution of iron(II) acetate and lithium methoxide in methanol. This synthesis produced a complex containing a novel three-dimensional lattice structure of iron and oxygen octahedra, which mimics several of the known structural features of Ft and ferrihydrite. The presence of both iron(II) and iron(III) cations distinguishes it from other known polynuclear iron oxo complexes. The X-ray structural, electronic and Mössbauer spectroscopic, and magnetic properties of **1** are described in this article, some aspects of which were previously reported in preliminary form.[15] Since **1** and the iron core of Ft are prepared in the same manner, by the oxidation of iron(II), the synthesis and properties of **1** may assist the interpretation of experiments that probe details of the biomineralization process occurring in the natural system.

Experimental Section

Ferrous acetate and a 1.6 M *n*-BuLi/hexane solution were purchased from Strem and Aldrich, respectively. All solvents, including MeOH, were distilled from appropriate drying agents under a dinitrogen atmosphere, except for the deuterated solvents CD_3OD and CD_2Cl_2, which were used as received after purging with Ar. All procedures were performed with strict exclusion of air, unless otherwise noted.

$[Fe_{12}(O)_2(OMe)_{18}(OAc)_6(MeOH)_{4.67}]$ (1). A methanol solution of LiOMe was prepared by careful addition of an *n*-BuLi/hexane solution to anhydrous methanol. Addition of 1 equiv of LiOMe (1.8 mL, 2.87 mmol) to 0.500 g (2.88 mmol, 1 equiv) of $Fe(OAc)_2$ suspended in MeOH produced a gray slurry. The volume of the mixture was adjusted to 20 mL, which corresponds to an iron concentration of approximately 0.14 M. After being stirred for several hours, the solution became light-green and a small amount of blue-green precipitate formed, which was removed by filtration. Dioxygen was added to the reaction solution by one of two methods. The solution could be sealed in a reaction flask under dinitrogen with a rubber septum and placed in a drying chamber filled with air. After at least 1 week, the solution became deep green and crystals of **1** formed. Alternatively, 1.0 mL of dioxygen, passed over anhydrous calcium sulfate and NaOH, could be added directly to the reaction solution. Vigorous shaking dissolved any green powder which initially formed, and after a few days, microcrystals of **1** were obtained. The slow diffusion method gave larger crystals of **1** than the rapid addition of dioxygen, and in both procedures a yellow powder also formed. Complex **1** was isolated under an inert atmosphere, and the contaminant was removed by slurrying and decanting with MeOH. The crystals decompose rapidly in dinitrogen or under vacuum. The average weight loss was 4.7(±0.2)%, which corresponds to the removal of 2.67 molecules of methanol. The vacuum-dried material therefore has the formula $[Fe_{12}(O)_2(OMe)_{18}(OAc)_6(MeOH)_2]$. For either method of preparation, approximately 0.040–0.070 g of **1** was obtained, the corresponding yield being 8–12% based on iron. Anal. Calcd for **1**, $C_{32}H_{80}O_{34}Fe_{12}$: C, 22.89; H, 4.80. Found: C, 22.55; H, 4.51. IR (KBr, cm^{-1}): 3240, 2925, 2813, 1560, 1414, 1344, 1077, 1025, 661, 480. Electronic spectrum in 50% CH_2Cl_2/50% MeOH or deuterated analogs [λ, nm (ε, M^{-1} cm^{-1})]: 1250 (sh), 900 (sh), 694 (2000), 338 (sh, 8200).

X-ray Crystallography. Crystals of **1** suitable for an X-ray diffraction study were obtained via the slow diffusion of dioxygen into the reaction solution. The rectangular block-shaped crystal examined had dimensions of 0.20 × 0.30 × 0.65 mm and was mounted on a quartz fiber with silicone grease. The average mean peak width, $\Delta\bar{\omega}_{1/2}$, for several low-angle reflections was somewhat broad, 0.37°, but the axial photographs revealed no fine structure, and the sample was deemed satisfactory. The Laue symmetry was found to be $\bar{1}$, and no higher symmetry was indicated by TRACER-II.[16] Data collection and reduction, including corrections for Lorentz and polarization effects, were performed by using general procedures previously described.[17] Initial iron positions were determined by using the direct methods program SHELXS-86.[18] The remainder of the heavy atoms were located from DIRDIF phase refinements[19] and difference Fourier maps, and the TEXSAN program package was used to refine the structure.[20] An absorption correction based on ψ scans was applied,[21] but no decay correction was necessary. All non-hydrogen atoms, except those involved in the static disorder model discussed below, were refined by anisotropic thermal parameters in the final solution. Hydrogen atoms bound to carbon were calculated by using a C–H distance of 0.95 Å, and the thermal parameters for the calculated hydrogen atoms were set equal to 1.2 × B_{eq} of the parent carbon atom. The two hydrogen atoms bound to oxygen atoms of methanol, H(1) and H(2), were located and refined isotropically. Several of the ligands for Fe(1) and Fe(6) were found to be disordered, and a two-site disorder model was applied. A chelating acetate, O(16), C(16), C(17), and O(17), which bridges Fe(6) and Fe(1), was refined isotropically with $^2/_3$ occupancy. A second acetate ligand, O(16), C(18), C(19), and O(18), is coordinated in a monodentate fashion to Fe(1), and a methanol ligand, O(19), and C(20), is bound to Fe(6). These two groups were also refined isotropically with $^1/_3$ occupancy. No hydrogen atoms were included in the refinement for any of the disordered carbon or oxygen atoms. The addition of the methanol ligand O(19) and C(20) with $^1/_3$ occupancy accounts for the nonintegral stoichiometry in the molecular formula of **1**. The largest shift/esd in the final cycle of refinement was 0.0004, and the largest peak in the final difference Fourier map was 1.15 e/Å^3 and was located near Fe(4). Crystallographic information is provided in Table 1, and final atom positional and equivalent isotropic thermal parameters are presented in Table 2. Anisotropic thermal parameters and a complete listing of bond distances and angles for **1** are available in the supplementary material.

Physical Measurements. Electronic spectra in the 300–900- and 500–1800-nm ranges were measured on Varian Lambda 7 and Cary 17D instruments, respectively. Fourier transform infrared spectra of KBr pellets were recorded on a Bio-Rad SPC3200 instrument. Mössbauer spectra of **1** mixed with BN were measured at a variety of temperatures using a conventional constant-acceleration spectrometer located at the Francis Bitter National Magnetic Laboratory. The γ-ray source, ^{57}Co in Rh, was maintained at room temperature. Isomer shifts were referenced to iron metal at 300 K.

(9) Only structurally characterized complexes having at least six iron atoms are included here. Fe_6: (a) Gérbéléu, N. V.; Batsanov, A. S.; Timko, G. A.; Struchkov, Y. T.; Indrichan, K. M.; Popovich, G. A. *Dokl. Akad. Nauk SSSR* **1987**, *293*, 122. (b) Micklitz, W.; Lippard, S. J. *Inorg. Chem.* **1988**, *27*, 3067. (c) Micklitz, W.; Bott, S. G.; Bentsen, J. G.; Lippard, S. J. *J. Am. Chem. Soc.* **1989**, *111*, 372. (d) Hegetschweiler, K.; Schmalle, H.; Streit, H. M.; Schneider, W. *Inorg. Chem.* **1990**, *29*, 3625. (e) McCusker, J. K.; Christmas, C. A.; Hagen, P. M.; Chadha, R. K.; Harvey, D. F.; Hendrickson, D. N. *J. Am. Chem. Soc.* **1991**, *113*, 6114. (f) Hegetschweiler, K.; Schmalle, H. W.; Streit, H. M.; Gramlich, V.; Hund, H.-U.; Erni, I. *Inorg. Chem.* **1992**, *31*, 1299. (g) Hagen, K. S.; Nair, V. S. *Inorg. Chem.* **1992**, *31*, 4048. (h) Harding, C. J.; Henderson, R. K.; Powell, A. K. *Angew. Chem., Int. Ed. Engl.* **1993**, *32*, 570.

(10) Fe_8: (a) Wieghardt, K.; Pohl, K.; Jibril, I.; Huttner, G. *Angew. Chem., Int. Ed. Engl.* **1984**, *23*, 77. (b) Delfs, C. D.; Gatteschi, D.; Pardi, L.; Sessoli, R.; Wieghardt, K.; Hanke, D. *Inorg. Chem.* **1993**, *32*, 3099.

(11) Fe_{10}: (a) Taft, K. L.; Lippard, S. J. *J. Am. Chem. Soc.* **1990**, *112*, 9629. (b) Taft, K. L.; Delfs, C. D.; Papaefthymiou, G. C.; Foner, S.; Gatteschi, D.; Lippard, S. J. *J. Am. Chem. Soc.* **1994**, *116*, 823.

(12) Fe_{11}: Gorun, S. M.; Papaefthymiou, G. C.; Frankel, R. B.; Lippard, S. J. *J. Am. Chem. Soc.* **1987**, *109*, 3337.

(13) $Fe_{16}M$, M = Mn(II), Co(II), or Fe(II): (a) Micklitz, W.; Lippard, S. J. *J. Am. Chem. Soc.* **1989**, *111*, 6856. (b) Micklitz, W.; McKee, V.; Rardin, R. L.; Pence, L. E.; Papaefthymiou, G. C.; Bott, S. G.; Lippard, S. J. Submitted for publication.

(14) Fe_{17}, Fe_{19}: Heath, S. L.; Powell, A. K. *Angew. Chem., Int. Ed. Engl.* **1992**, *31*, 191.

(15) Taft, K. L.; Papaefthymiou, G. C.; Lippard, S. J. *Science* **1993**, *259*, 1302.

(16) Lawton, S. L. *TRACER II: A Fortran Lattice Transformation-Cell Reduction Program*; Mobil Oil Corp.: Paulsboro, NJ, 1967.

(17) Carnahan, E. M.; Rardin, R. L.; Bott, S. G.; Lippard, S. J. *Inorg. Chem.* **1992**, *31*, 5193.

(18) Sheldrick, G. M. In *Crystallographic Computing*; Sheldrick, G. M., Krüger, C., Goddard, R., Eds.; Oxford University Press: Oxford, U.K., 1985; pp 175 ff.

(19) Pathasarathi, V.; Beurskens, P. T.; Slot, J. J. B. *Acta Crystallogr.* **1983**, *A39*, 860.

(20) *TEXSAN: Single Crystal Structure Analysis Software, Version 5.0*; Molecular Structure Corp.: The Woodlands, TX, 1989.

(21) North, A. C. T.; Phillips, D. C.; Mathews, F. S. *Acta Crystallogr.* **1968**, *A24*, 351.

Table 1. Crystallographic Information for $[Fe_{12}(O)_2(OMe)_{18}(OAc)_6(MeOH)_{4.67}]$ (1)[a]

formula	$Fe_{12}C_{34.67}H_{90.67}O_{36.67}$
fw	1764.67
cryst syst	triclinic
space group[b]	$P\bar{1}$ (No. 2)
a, Å	11.868(2)
b, Å	13.309(2)
c, Å	10.437(2)
α, deg	100.96(2)
β, deg	95.30(2)
γ, deg	80.07(1)
V, Å^3	1591.2(5)
Z	1
d_{calcd}, g cm^{-3}	1.841
T, K	185
data collctn range, deg	$3 \le 2\theta \le 54$
data limits	$+h,\pm k,\pm l$
no. of data collected	7570
R_{av}	0.021
no. of unique data	6912
no. obs unique data[c]	4709
no. of parameters	383
data/parameter ratio	12.3
abs coeff, cm^{-1}	27.4
transm coeff, min/max	0.89/1.00
R^d	0.054
R_w	0.071
largest shift/esd, final	0.0004
largest peak, e/Å^3	1.15

[a] All measurements were made by using an Enraf-Nonius CAD-4F κ-geometry diffractometer and Mo Kα (0.710 69 Å) radiation. [b] Hahn, T., Ed. *International Tables for X-ray Crystallography*, D. Reidel: Dordrecht, The Netherlands, 1983. [c] Observation criterion: $I > 3\sigma(I)$. [d] $R = \sum||F_o| - |F_c||/\sum|F_o|$, and $R_w = [\sum w(|F_o| - |F_c|)^2/\sum w|F_o|^2]^{1/2}$, where $w = 1/\sigma^2(F)$ and $\sigma^2(F)$ is defined in ref 17.

Solid-state magnetic measurements of **1** (0.0354 g) were made with a Quantum Design SQUID susceptometer located in the Department of Material Science and Engineering at MIT. Fifty-three data points between 2.5 and 300 K were collected at 5 kG. The magnetism of the sample holder was measured at the same field and temperatures and subtracted from the values found for **1**. A diamagnetic correction of -7.9×10^{-4} for **1** was calculated from Pascal's constants and applied.[22] Dc magnetization studies of **1** at 1.4 K from 0 to 20 T were performed at the Francis Bitter National Magnet Laboratory. A vibrating-sample magnetometer adapted for use with a Bitter electromagnet was used.[23] A sample of **1**, weighing 0.0108 g, was restrained in a Teflon bucket with a plunger rod. No corrections were made for the negligible magnetic contributions to the magnetization values of the sample holder nor the inherent diamagnetism of the atoms.

Results and Discussion

Synthesis. Most polynuclear iron oxo complexes have been prepared from iron(III) reagents by self-assembly reactions.[3,9-14] Through judicious control of reagents, solvents, and stoichiometry, complexes containing up to 19 ferric ions have been isolated and characterized by X-ray crystallography. Iron–oxo–hydroxo particles with extended structures have been prepared upon hydrolysis of simple iron(III) salts, the "Spiro–Saltman ball" being a well-known example.[24] By contrast, only a few complexes have been prepared from iron(II) starting materials. One mixed-valent polyiron oxo complex, $[Fe^{II}Fe_{16}^{III}(O)_{10}(OH)_{10}(OBz)_{20}]$ (**2**), was isolated upon air oxidation of reduced basic iron benzoate $[Fe^{II}Fe_2^{III}(O)(OBz)_6(OH_2)_3]$.[13b] A hexanuclear iron(III) complex, $[Fe_6(O)_2(OMe)_6(tren)_2]$,[25] was generated from ferrous triflate and tren in methanol upon exposure to air.[9g] Given that the iron–oxo–hydroxo core of ferritin is prepared in vitro from aqueous ferrous ions upon air oxidation, we decided to react iron(II) carboxylates with dioxygen under basic conditions as a potential route to new model complexes. Methanol rather than water was used as solvent to avoid the precipitation of iron hydroxides.

Air oxidation of ferrous acetate and lithium methoxide in methanol ultimately produces an intractable yellow solid. The precipitate contained bridging methoxide and acetate ligands, as indicated by IR spectroscopy, and was most likely polymeric in nature. A number of polyiron(III) alkoxide carboxylate complexes have been described in the literature, but their structures are unknown.[26] One exception is the decanuclear iron(III) complex $[Fe(OMe)_2(O_2CCH_2Cl)]_{10}$, known as a molecular "ferric wheel" because of its circular structure.[11] During the oxidation reaction of ferrous acetate, a blue-green powder formed, and further exposure to air afforded the yellow powder.

Complex **1** was crystallized directly from the reaction mixture upon the slow diffusion of air or the introduction of small amounts of dioxygen. The diffusion method provided deep green crystals after a few weeks, whereas exposure to dioxygen afforded smaller

Table 2. Final Atom Positional and Equivalent Isotropic Thermal Parameters for $[Fe_{12}(O)_2(OMe)_{18}(OAc)_6(MeOH)_{4.67}]$ (1)[a]

atom	x	y	z	B_{eq},[b] Å^2
Fe(1)	0.28244(8)	0.69189(7)	−0.08187(9)	1.54(4)
Fe(2)	0.42342(7)	0.74332(7)	0.18463(8)	1.38(4)
Fe(3)	0.57339(7)	0.52800(7)	0.13909(8)	1.24(3)
Fe(4)	0.54281(7)	0.68205(7)	−0.06820(8)	1.37(4)
Fe(5)	0.70292(7)	0.45280(7)	−0.13105(8)	1.31(3)
Fe(6)	0.84107(9)	0.21249(8)	−0.1808(1)	2.82(5)
O	0.4133(3)	0.6244(3)	0.0325(4)	1.2(2)
O(1)	0.2865(4)	0.5650(3)	−0.2066(4)	1.7(2)
O(2)	0.2880(4)	0.8149(3)	0.0745(4)	2.0(2)
O(3)	0.5427(4)	0.6617(3)	0.2783(4)	1.7(2)
O(4)	0.3987(4)	0.7442(4)	−0.1626(4)	2.1(2)
O(5)	0.5319(4)	0.7976(3)	0.0969(4)	1.8(2)
O(6)	0.5493(4)	0.5366(3)	−0.2022(4)	1.4(2)
O(7)	0.6704(3)	0.5826(3)	0.0230(4)	1.5(2)
O(8)	0.7038(4)	0.3121(3)	−0.2628(4)	1.7(2)
O(9)	0.8255(4)	0.3531(3)	−0.0355(4)	1.7(2)
O(10)	0.6686(5)	0.7202(4)	−0.1747(5)	2.8(2)
O(11)	0.9641(6)	0.2523(6)	−0.282(1)	6.1(4)
O(12)	0.8002(4)	0.5369(4)	−0.2224(5)	2.4(2)
O(13)	0.9480(5)	0.4374(5)	−0.3251(6)	3.9(3)
O(14)	0.3952(4)	0.8716(4)	0.3274(4)	2.3(2)
O(15)	0.2035(4)	0.9078(4)	0.3300(6)	3.3(2)
O(16)	0.1494(4)	0.7742(4)	−0.1670(5)	2.6(2)
O(17)	0.0479(7)	0.8528(6)	0.0211(8)	3.0(2)
O(18)	−0.022(2)	0.871(2)	−0.133(2)	4.4(4)
O(19)	0.017(1)	0.872(1)	0.119(1)	2.4(3)
C(1)	0.2296(6)	0.5534(6)	−0.3320(7)	2.4(3)
C(2)	0.2908(7)	0.9168(6)	0.0496(8)	3.2(4)
C(3)	0.6128(6)	0.7047(6)	0.3841(6)	2.4(3)
C(4)	0.3854(7)	0.8096(6)	−0.2555(7)	3.0(4)
C(5)	0.5806(7)	0.8882(6)	0.1364(8)	3.3(4)
C(6)	0.5327(6)	0.5445(5)	−0.3383(6)	1.9(3)
C(7)	0.7630(6)	0.6313(5)	0.0906(7)	2.1(3)
C(8)	0.7004(7)	0.3117(6)	−0.4004(7)	2.6(3)
C(9)	0.9301(6)	0.3876(6)	0.0204(7)	2.3(3)
C(10)	0.705(1)	0.8108(8)	−0.184(1)	8.1(7)
C(11)	1.045(2)	0.189(1)	−0.356(3)	24(2)
C(12)	0.8833(6)	0.5191(6)	−0.3001(7)	2.4(3)
C(13)	0.8981(7)	0.6074(7)	−0.3636(7)	3.1(4)
C(14)	0.3018(7)	0.9239(6)	0.3696(7)	2.7(3)
C(15)	0.3142(8)	1.0123(7)	0.481(1)	4.5(4)
C(16)	0.067(1)	0.840(1)	−0.105(1)	3.3(2)
C(17)	−0.007(1)	0.908(1)	−0.183(2)	4.3(3)
C(18)	0.064(2)	0.829(2)	−0.213(2)	2.4(4)
C(19)	0.039(2)	0.846(2)	−0.344(3)	3.8(5)
C(20)	−0.094(2)	0.896(2)	0.159(3)	3.7(5)
H(1)	0.708(6)	0.659(5)	−0.191(7)	2(2)
H(2)	0.964(8)	0.311(7)	−0.31(1)	4(2)

[a] Numbers in parentheses are errors in the last significant digit. [b] $B_{eq} = {}^4/_3[a^2\beta_{11} + b^2\beta_{22} + c^2\beta_{33} + 2ab(\cos\gamma)\beta_{12} + 2ac(\cos\beta)\beta_{13} + 2bc(\cos\alpha)\beta_{23}]$.

(22) (a) O'Connor, C. J. *Prog. Inorg. Chem.* **1982**, *29*, 203. (b) Carlin, R. L. *Magnetochemistry*; Springer-Verlag: New York, 1986.
(23) Foner, S. *Rev. Sci. Instrum.* **1959**, *30*, 548.
(24) Spiro, T. G.; Allerton, S. E.; Renner, J.; Terzis, A.; Bils, R.; Saltman, P. *J. Am. Chem. Soc.* **1966**, *88*, 2721.

(25) Abbreviations: HDPM, dipivaloylmethane; tren, tris(2-aminoethyl)-amine.

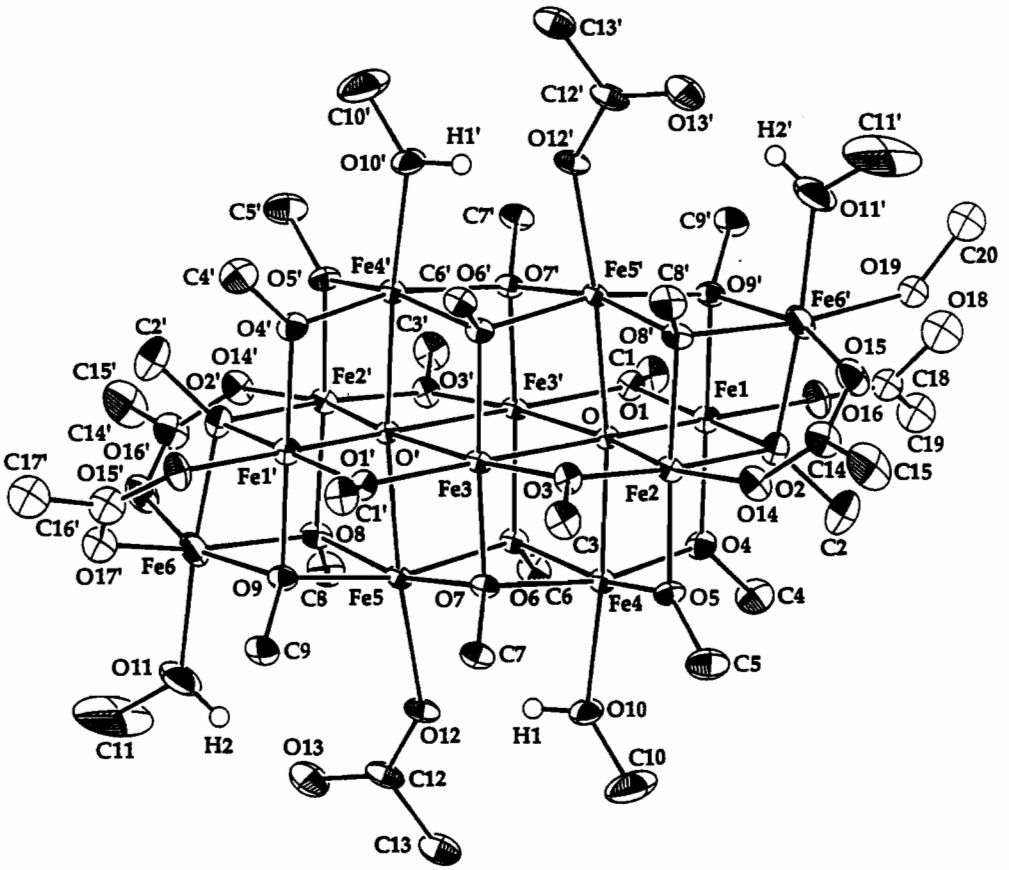

Figure 1. ORTEP depiction of **1** displaying the 40% probability thermal ellipsoids. Hydrogen atoms bound to carbon are omitted for clarity. Primed and unprimed atoms are related by a crystallographically-imposed center of symmetry, and only one symmetry-related set is depicted for the two disorder models (see text).

crystals of **1** in just 1–2 days. A small amount of yellow powder also formed. The yield of **1** was quite low, below 15% based on iron, but the low solubility of the complex and the limited amount of dioxygen which can be introduced decreased the efficiency of the procedure. A similar oxidation technique was used to prepare a mixed-valent, tetranuclear iron cube $[Fe_4(OMe)_5(MeOH)_3(OBz)_4]$ (**3**).[27] Magnetite was similarly produced within the Ft protein cavity upon the careful addition of small aliquots of air to iron(II) and the apoprotein.[28]

Samples of **1** were collected under an inert atmosphere owing to their air sensitivity. Any yellow contaminant formed in the generation of **1** was separated by decanting the mixture with methanol. Crystals of **1** decomposed while standing in dinitrogen or under vacuum. From the measured weight loss, the most likely formula for the resultant green powder is $[Fe_{12}(O)_2(OMe)_{18}(OAc)_6(MeOH)_2]$.

Alkoxide ligands were used recently in order to prepare discrete, high-nuclearity iron–oxygen complexes, for they can both bridge metal ions and terminate cluster growth.[9d,f,g,11,27] Although they have different chemical reactivities, the characteristic coordination properties of alkoxide and hydroxide ligands are similar, and the methoxide bridges in **1** mimic the hydroxide ligation present in aqueous systems. Alkoxide ligands can bridge at most three metal ions. Oxo anions, which are capable of bridging up to six metal ions, generally increase the metal nuclearity and often result in polymeric or extended structures. Oxo ligands are most commonly provided by reduction of dioxygen or by deprotonation of coordinated water. The low dioxygen concentration and dry experimental conditions employed in the synthesis of **1** limited the available number of oxo ligands, and probably contributed to our ability to isolate a discrete cluster.

Structural Study. An ORTEP view of **1** is given in Figure 1. The compound resides on a crystallographically imposed center of symmetry, relating the primed and unprimed atoms. Atoms having an occupancy of less than 1, O(17)–O(19) and C(16)–C(20), are drawn as cross-hatched spheres, and the two hydrogen atoms H(1) and H(2) are shown as open spheres. For clarity, only one set, either primed or unprimed, of the disordered atoms is drawn. Selected bond distances and angles for complex **1** are listed in Table 3, and the Fe···Fe distances for edge-shared octahedra are listed in Table 4.

A key structural element in the complex is the two central μ_6-oxo ligands, O and O′, which together link ten iron atoms. Two additional iron atoms, Fe(6) and Fe(6)′, are not attached to the oxo anions. Bridging methoxide ligands, of both the μ_2-OMe and μ_3-OMe variety, complete the coordination spheres of the iron atoms in the $\{Fe_{12}(O)_2(OMe)_{18}\}^{6+}$ core. The terminal positions of this core are occupied by acetate, either bidentate bridging or monodentate terminal, and methanol ligands. All the metal ions are coordinated by six oxygen donor ligands and have approximately pseudooctahedral geometry. As evident from Figure 2, the iron–oxygen framework has a distorted sodium chloride structure. The oxygen atoms are packed in a face-centered cubic arrangement with iron atoms occupying octahedral interstices. The layers of iron and oxygen atoms present in the $\{Fe_{12}(O)_2(OMe)_{18}\}^{6+}$ core are highlighted in Figure 3.

From charge considerations, we assign four of the iron atoms in **1** as iron(III) and the remainder as iron(II) ions. Atoms Fe(1), Fe(1)′, Fe(2), and Fe(2)′ are assigned as iron(III) on the basis of bond distance comparisons. The average Fe–O bond lengths for these sites is 2.02 Å, whereas the other eight iron(II) atoms have average Fe–O distances ranging from 2.12 to 2.2 Å. The assignment of the ferric sites in **1** is perhaps most convincing when the Fe–μ_6-O bond lengths are considered. The Fe(1)–μ_6-O

(26) (a) Kokot, E.; Mockler, G. M.; Sefton, G. L. *Aust. J. Chem.* **1973**, *26*, 2105. (b) Trzeciak, A.; Szymanska-Buzar, T.; Ziolkowski, J. J. *Polish J. Chem.* **1979**, *53*, 981.
(27) Taft, K. L.; Caneschi, A.; Pence, L. E.; Delfs, C. D.; Papaefthymiou, G. C.; Lippard, S. J. *J. Am. Chem. Soc.* **1993**, *115*, 11753.
(28) Meldrum, F. C.; Heywood, B. R.; Mann, S. *Science* **1992**, *257*, 522.

Table 3. Selected Bond Distances (Å) and Angles (deg) for $[Fe_{12}(O)_2(OMe)_{18}(OAc)_6(MeOH)_{4.67}]$ (**1**)[a]

Fe(1)–O	2.056(4)	Fe(3)–O(3)	2.074(4)	Fe(5)–O(6)	2.117(4)
Fe(1)–O(1)	1.922(4)	Fe(3)–O(6)′	2.029(4)	Fe(5)–O(7)	2.133(4)
Fe(1)–O(2)	2.086(4)	Fe(3)–O(7)	2.050(4)	Fe(5)–O(8)	2.101(4)
Fe(1)–O(4)	1.967(5)	Fe(3)–O	2.409(4)	Fe(5)–O(9)	2.108(5)
Fe(1)–O(9)′	2.082(4)	Fe(3)–O′	2.430(4)	Fe(5)–O(12)	2.132(5)
Fe(1)–O(16)	1.999(5)	Fe(4)–O	2.251(4)	Fe(6)–O(2)′	2.091(5)
Fe(2)–O	2.029(4)	Fe(4)–O(4)	2.023(5)	Fe(6)–O(8)	2.138(5)
Fe(2)–O(2)	2.088(5)	Fe(4)–O(5)	2.078(4)	Fe(6)–O(9)	2.165(5)
Fe(2)–O(3)	1.939(4)	Fe(4)–O(6)	2.156(4)	Fe(6)–O(11)	2.072(7)
Fe(2)–O(5)	1.951(4)	Fe(4)–O(7)	2.114(4)	Fe(6)–O(15)′	2.111(5)
Fe(2)–O(8)′	2.080(4)	Fe(4)–O(10)	2.122(5)	Fe(6)–O(17)′	2.240(8)
Fe(2)–O(14)	2.043(4)	Fe(5)–O′	2.274(4)	Fe(6)–O(19)′	1.99(1)
Fe(3)–O(1)′	2.049(4)				
O–Fe(1)–O(1)	91.1(2)	O(3)–Fe(3)–O(7)	97.6(2)	Fe(3)–O–Fe(5)′	87.5(1)
O–Fe(1)–O(2)	81.0(2)	O(6)′–Fe(3)–O(7)	162.8(7)	Fe(3)′–O–Fe(4)	88.1(1)
O–Fe(1)–O(4)	87.9(2)	O–Fe(4)–O(4)	81.4(2)	Fe(3)′–O–Fe(5)′	87.1(1)
O–Fe(1)–O(9)′	85.2(2)	O–Fe(4)–O(5)	82.1(2)	Fe(4)–O–Fe(5)′	173.0(2)
O–Fe(1)–O(16)	170.8(2)	O–Fe(4)–O(6)	85.5(1)	O(2)′–Fe(6)–O(8)	83.3(2)
O(1)–Fe(1)–O(2)	171.1(2)	O–Fe(4)–O(7)	87.2(2)	O(2)′–Fe(6)–O(9)	80.5(2)
O(1)–Fe(1)–O(4)	95.1(2)	O–Fe(4)–O(10)	173.9(2)	O(2)′–Fe(6)–O(11)	175.4(2)
O(1)–Fe(1)–O(9)′	92.8(2)	O(4)–Fe(4)–O(5)	95.5(2)	O(2)′–Fe(6)–O(15)′	87.6(2)
O(1)–Fe(1)–O(16)	97.5(2)	O(4)–Fe(4)–O(6)	91.7(2)	O(2)′–Fe(6)–O(17)′	81.5(2)
O(2)–Fe(1)–O(4)	88.6(2)	O(4)–Fe(4)–O(7)	164.7(2)	O(2)′–Fe(6)–O(19)′	104.7(4)
O(2)–Fe(1)–O(9)′	82.6(2)	O(4)–Fe(4)–O(10)	100.0(2)	O(8)–Fe(6)–O(9)	76.9(2)
O(2)–Fe(1)–O(16)	90.2(2)	O(5)–Fe(4)–O(6)	164.6(2)	O(8)–Fe(6)–O(11)	93.6(3)
O(4)–Fe(1)–O(9)′	169.6(2)	O(5)–Fe(4)–O(7)	93.0(2)	O(8)–Fe(6)–O(15)′	86.8(2)
O(4)–Fe(1)–O(16)	94.5(2)	O(5)–Fe(4)–O(10)	103.6(2)	O(8)–Fe(6)–O(17)′	156.2(2)
O(9)′–Fe(1)–O(16)	91.1(2)	O(6)–Fe(4)–O(7)	77.2(2)	O(8)–Fe(6)–O(19)′	171.9(4)
O–Fe(2)–O(2)	81.6(2)	O(6)–Fe(4)–O(10)	88.5(2)	O(9)–Fe(6)–O(11)	95.5(2)
O–Fe(2)–O(3)	92.7(2)	O(7)–Fe(4)–O(10)	90.3(2)	O(9)–Fe(6)–O(15)′	160.7(2)
O–Fe(2)–O(5)	91.3(2)	O′–Fe(5)–O(6)	85.5(1)	O(9)–Fe(6)–O(17)′	82.7(2)
O–Fe(2)–O(8)′	86.0(2)	O′–Fe(5)–O(7)	86.6(1)	O(9)–Fe(6)–O(19)′	103.3(4)
O–Fe(2)–O(14)	167.1(2)	O′–Fe(5)–O(8)	79.6(2)	O(11)–Fe(6)–O(15)′	95.7(3)
O(2)–Fe(2)–O(3)	173.3(2)	O′–Fe(5)–O(9)	79.4(2)	O(11)–Fe(6)–O(17)′	100.4(3)
O(2)–Fe(2)–O(5)	89.9(2)	O′–Fe(5)–O(12)	174.9(2)	O(11)–Fe(6)–O(19)′	78.3(5)
O(2)–Fe(2)–O(8)′	84.8(2)	O(6)–Fe(5)–O(7)	77.6(2)	O(15)′–Fe(6)–O(17)′	110.6(3)
O(2)–Fe(2)–O(14)	87.1(2)	O(6)–Fe(5)–O(8)	99.0(2)	O(15)′–Fe(6)–O(19)′	94.4(4)
O(3)–Fe(2)–O(5)	93.7(2)	O(6)–Fe(5)–O(9)	164.9(2)	Fe(1)–O(1)–Fe(3)′	102.9(2)
O(3)–Fe(2)–O(8)′	91.4(2)	O(6)–Fe(5)–O(12)	90.0(2)	Fe(1)–O(2)–Fe(2)	97.3(2)
O(3)–Fe(2)–O(14)	98.2(2)	O(7)–Fe(5)–O(8)	166.1(2)	Fe(1)–O(2)–Fe(6)′	98.8(2)
O(5)–Fe(2)–O(8)′	174.4(2)	O(7)–Fe(5)–O(9)	100.7(2)	Fe(2)–O(2)–Fe(6)′	95.4(2)
O(5)–Fe(2)–O(14)	94.9(2)	O(7)–Fe(5)–O(12)	90.1(2)	Fe(2)–O(3)–Fe(3)	100.2(2)
O(8)′–Fe(2)–O(14)	86.8(2)	O(8)–Fe(5)–O(9)	78.9(2)	Fe(1)–O(4)–Fe(4)	100.2(2)
O–Fe(3)–O′	94.9(1)	O(8)–Fe(5)–O(12)	103.5(2)	Fe(2)–O(5)–Fe(4)	97.0(2)
O–Fe(3)–O(1)′	172.7(2)	O(9)–Fe(5)–O(12)	105.1(2)	Fe(3)′–O(6)–Fe(4)	102.2(2)
O–Fe(3)–O(3)	79.2(2)	Fe(1)–O–Fe(2)	100.2(2)	Fe(3)′–O(6)–Fe(5)	102.7(2)
O–Fe(3)–O(6)′	84.0(2)	Fe(1)–O–Fe(3)	172.0(2)	Fe(4)–O(6)–Fe(5)	100.6(2)
O–Fe(3)–O(7)	84.6(2)	Fe(1)–O–Fe(3)′	87.2(1)	Fe(3)–O(7)–Fe(4)	100.8(2)
O′–Fe(3)–O(1)′	78.3(2)	Fe(1)–O–Fe(4)	90.5(2)	Fe(3)–O(7)–Fe(5)	101.6(2)
O′–Fe(3)–O(3)	173.5(2)	Fe(1)–O–Fe(5)′	94.4(2)	Fe(4)–O(7)–Fe(5)	101.5(2)
O′–Fe(3)–O(6)′	83.8(1)	Fe(2)–O–Fe(3)	87.5(1)	Fe(2)′–O(8)–Fe(5)	98.4(2)
O′–Fe(3)–O(7)	84.4(1)	Fe(2)–O–Fe(3)′	172.3(2)	Fe(2)′–O(8)–Fe(6)	94.2(2)
O(1)′–Fe(3)–O(3)	107.7(2)	Fe(2)–O–Fe(4)	89.5(1)	Fe(5)–O(8)–Fe(6)	102.3(2)
O(1)′–Fe(3)–O(6)′	97.8(2)	Fe(2)–O–Fe(5)′	94.5(2)	Fe(1)′–O(9)–Fe(5)	98.8(2)
O(1)′–Fe(3)–O(7)	92.0(2)	Fe(3)–O–Fe(3)′	85.1(1)	Fe(1)′–O(9)–Fe(6)	96.6(2)
O(3)–Fe(3)–O(6)′	92.8(2)	Fe(3)–O–Fe(4)	87.0(1)	Fe(5)–O(9)–Fe(6)	101.2(2)

[a] Numbers in parentheses are estimated standard deviations in the last significant digit. Primed and unprimed atoms are related by the crystallographically-imposed center of symmetry.

Table 4. Edge-Shared Fe···Fe Distances (Å) in $[Fe_{12}(O)_2(OMe)_{18}(OAc)_6(MeOH)_{4.67}]$ (**1**)[a]

Fe(1)···Fe(2)	3.133(1)	Fe(2)···Fe(6)′	3.090(1)
Fe(1)···Fe(3)′	3.106(1)	Fe(3)···Fe(3)′	3.273(2)
Fe(1)···Fe(4)	3.061(1)	Fe(3)···Fe(4)	3.210(1)
Fe(1)···Fe(5)′	3.181(1)	Fe(3)···Fe(4)′	3.259(1)
Fe(1)···Fe(6)′	3.172(2)	Fe(3)···Fe(5)	3.242(1)
Fe(2)···Fe(3)	3.080(1)	Fe(3)···Fe(5)′	3.239(1)
Fe(2)···Fe(4)	3.018(1)	Fe(4)···Fe(5)	3.289(1)
Fe(2)···Fe(5)′	3.165(1)	Fe(5)···Fe(6)	3.302(1)

[a] Numbers in parentheses are estimated standard deviations in the last significant digit. Primed and unprimed atoms are related by the crystallographically-imposed center of symmetry.

and Fe(2)–μ_6-O bond distances are at least 0.2 Å shorter than the Fe(4)–μ_6-O or Fe(5)–μ_6-O distances and more than 0.35 Å shorter than the corresponding Fe(3)–μ_6-O and Fe(3)′–μ_6-O distances. The effects of these inequalities can be appreciated

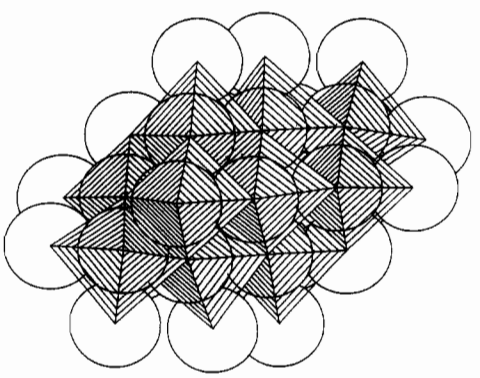

Figure 2. View of the distorted face-centered cubic lattice in **1**, showing the oxygen atoms (open spheres) and the 12 iron ions (cross-hatched octahedra).

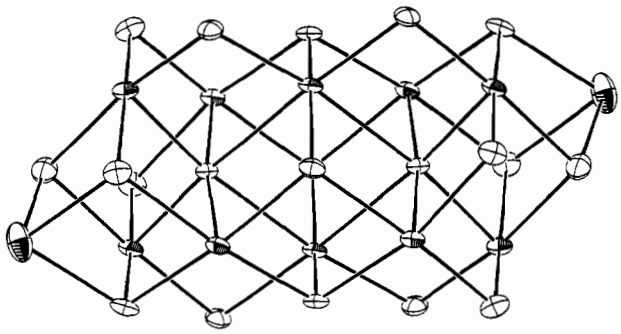

Figure 3. Layers of iron and oxygen atoms in **1**. The metal ions are drawn as heavily shaded ellipses, and the oxygen atoms have a single cross-hatch, with only the bridging oxygen atoms included. The view shown is taken along the vector joining O(7) and O(7)′ (see Figure 1).

in Figure 1, where it can be readily seen that the μ_6-O and μ_6-O′ atoms are shifted toward the ferric positions.

The exterior coordination sites of the $\{Fe_{12}(O)_2(OMe)_{18}\}^{6+}$ core are occupied by acetate and methanol ligands. The monodentate acetate ligand O(12), C(12), C(13), and O(13) and the two methanol ligands O(10), C(10), O(11), and C(11) are intramolecularly hydrogen bonded. The distances between oxygen atoms are 2.647(7) Å for O(10)···O(12) and 2.56(1) Å for O(11)···O(13), values indicative of relatively strong interactions. Terminal carboxylate ligands often form weak hydrogen bonds with their noncoordinated oxygen atoms, but hydrogen-bonding interactions with both oxygen atoms of a coordinated carboxylate anion are unusual.[29] Chelating acetates also bridge the terminal sites. One such ligand, O(14), C(14), C(15), and O(15), refined well, whereas the other, O(16), C(16), C(17), and O(17), had unusually large thermal parameters and unreasonable bond distances and angles. The model was therefore modified to account for the electron density at this site. A monodentate acetate bound to Fe(1) [O(16), C(18), C(19), and O(18)], which is hydrogen bonded to a methanol ligand [O(19) and O(20)] coordinated to Fe(6)′ (Figure 1), was introduced. The O(18)···O(19) distance of 2.63(3) Å is in good agreement with distances found for the other hydrogen-bonded interactions in the molecule. These atoms were refined isotropically with $^1/_3$ occupancy, and the bridging acetate [O(16), C(16), C(17), and O(17)] was also refined isotropically with an occupancy of $^2/_3$. This ratio preserves the charge balance in **1**, although resulting in a nonintegral amount of methanol in the molecular formula.

The $\{Fe_{12}(O)_2(OMe)_{18}\}^{6+}$ core of **1** is considerably distorted from the positions of an idealized face-centered cubic lattice. Inequivalent Fe–O bond lengths occur as a result of the two different iron oxidation states, and additional structural perturbations arise from the presence of both doubly and triply bridging methoxide ligands. The Fe–μ_2-OMe bond lengths are 0.14 and 0.05 Å shorter for iron(III) and iron(II), respectively, than their Fe–μ_3-OMe counterparts, as indicated in Table 5. A similar inverse relationship between coordination number and the metal–oxygen distance has been noted for other polyiron oxo complexes.[9,13] The Fe···Fe distances at edge-shared sites in **1** vary from 3.02 to 3.30 Å, reflecting the substantial distortions in the core.

A unit cell packing diagram is supplied in Figure 4. The second disorder model, consisting of a monodentate acetate and methanol ligands, is depicted in this stereoscopic view.

Structural Comparisons. The structure of **1** is related to a large number of polymetallic species, including polyiron–oxygen complexes,[3,9-14] early-transition-metal polyoxometalates,[30] iron oxides,[4] mixed-valent iron-containing minerals,[31] and of course Ft and ferrihydrite.[6,8] Only one other discrete polyiron oxo structural motif has μ_6-oxo bridges like those present in **1**, namely, the $\{Fe^{III}_6(\mu_6\text{-}O)(OR)_{18}\}^{2-}$ core found in both $[Fe_6O\{(OCH_2)_3CMe\}_6]^{2-}$ (**4**) and $[Fe_6O(OMe)_{18}]^{2-}$ (**5**).[9d,f] Since other high-nuclearity polyiron complexes lack this structural element, they exhibit either a layered or globular iron–oxygen array, instead of a lattice framework. Complex **1** and its relatives **4** and **5** are therefore unique entries to this class. The Fe–μ_6-O distances in the hexanuclear iron complexes **4** and **5** are much more regular than those in **1** owing to the uniform oxidation state of the iron atoms, as indicated in Table 5. The Fe(III)–μ_6-O distances in **1** are much shorter in order to compensate for the long Fe(II)–μ_6-O bond lengths. The sources of the oxo anions also differ for the molecules. In **4** and **5**, the μ_6-oxo ligand arises from water, whereas for **1** the oxo anions most likely originate from reduction of dioxygen.

The distorted face-centered cubic lattice in **1** can be subdivided into four $\{Fe_4(O)_n(OR)_{4-n}\}$ cubes. The cubane architecture was only recently realized for iron with oxygen bridging atoms.[27,32] Two discrete tetranuclear iron(II) methoxide cubes having the molecular formula $[Fe(OMe)(MeOH)L]_4$, where HL is either dipivaloylmethane (**6**) or dibenzoylmethane (**7**), and the mixed-valent cube **3** have been prepared.[27] The Fe–O bond lengths in these iron–methoxide cubes are quite similar to those found for **1** (Table 5).

The metal–oxygen core adopted in **1** is a classical structural motif found in early-transition-metal polyoxometalates.[30] A familiar example is $[V_{10}O_{28}]^{6-}$, in which ten vanadium(V) ions are bridged by two μ_6-oxo ligands.[33] Reduced vanadium derivatives having the same metal–oxygen core in both V(IV) and V(V) oxidation states have been prepared by using the chelating ligand $RC(CH_2O)_3^{3-}$, also present in **4**.[34] A mixed-valent manganese(II,III) complex, $[Mn_{10}(O)_2Cl_8\{(OCH_2)_3CMe\}_6]^{2-}$, was also recently reported.[35]

As observed for the polyoxometalates, **1** has structural features reminiscent of metal oxides with extended lattices.[4] One closely related iron oxide is wüstite, which has a defect sodium chloride structure and an approximate formula of FeO. Pure wüstite is metastable and is therefore more accurately represented as $Fe(II)_{1-3x}Fe(III)_{2x}O$, with $(1-x)$ usually between 0.84 and 0.95. The ferrous ions occupy octahedral sites, with iron(III) defects located in tetrahedral interstices. The all-iron(III) mineral lepidocrocite, γ-FeOOH, also has a cubic close-packed oxygen lattice. In this case, however, the ferric ions occupy octahedral positions. Double chains of edge-shared iron and oxygen octahedra form a layered structure, with the protons situated between the iron–oxygen sheets.

Many mixed-valence iron-containing minerals have been structurally characterized, and representatives with edge-shared iron octahedra are known.[31] One example, babingtonite, which has the composition $\{Ca_2Fe^{II}Fe^{III}Si_5O_{14}(OH)\}$, consists of a tetramer of two edge-shared iron(II) ions with an iron(III) cation at both ends. Although none of these mixed-valent minerals has a close-packed array of oxygen atoms, they and complex **1** are similar in that they have exclusive oxygen atom coordination and contain both iron(II) and iron(III).

Unlike the structures of these other crystalline solids, the structure of the polyiron core in Ft and the related mineral ferrihydrite is still in question.[6] Only low-resolution X-ray powder diffraction data are available for these iron–oxo–hydroxo species because of their poor crystallinity. Several models for the structure of the Ft inorganic core and the closely related mineral ferrihydrite have been advanced. The generally accepted ferrihydrite structure

(29) (a) Rardin, R. L.; Tolman, W. B.; Lippard, S. J. *New J. Chem.* **1991**, *15*, 417. (b) Ménage, S.; Que, L., Jr. *Inorg. Chem.* **1990**, *29*, 4293.
(30) (a) Day, V. W.; Klemperer, W. G. *Science* **1985**, *228*, 533. (b) Pope, M. T.; Müller, A. *Angew. Chem., Int. Ed. Engl.* **1991**, *30*, 34.
(31) (a) Burns, R. G. *Annu. Rev. Earth Planet. Sci.* **1981**, *9*, 345. (b) Amthauer, G.; Rossman, G. R. *Phys. Chem. Miner.* **1984**, *11*, 37.
(32) Shoner, S. C.; Power, P. P. *Inorg. Chem.* **1992**, *31*, 1001.
(33) Evans, H. T., Jr. *Inorg. Chem.* **1966**, *5*, 967.
(34) (a) Khan, M. I.; Chen, Q.; Goshorn, D. P.; Hope, H.; Parkin, S.; Zubieta, J. *J. Am. Chem. Soc.* **1992**, *114*, 3341. (b) Khan, M. I.; Chen, Q.; Goshorn, D. P.; Zubieta, J. *Inorg. Chem.* **1993**, *32*, 672.
(35) Cavaluzzo, M.; Chen, Q.; Zubieta, J. *J. Chem. Soc., Chem. Commun.* **1993**, 131.

Table 5. Comparison of Selected Interatomic Distances (Å) for Polynuclear Iron–Alkoxide Complexes[a]

	1[b]		3		5		6	
structural parameter	range	avg	range	avg	range	avg	range	avg
Fe–μ_6–O	2.03–2.43	2.2(2)	*c*	*c*	2.25–2.30	2.29(2)	*c*	*c*
Fe(III)–μ_2–OMe	1.92–1.97	1.94(2)	*c*	*c*	1.95–2.03	2.00(3)	*c*	*c*
Fe(II)–μ_2–OMe	2.02–2.08	2.06(3)	*c*	*c*	*c*	*c*	*c*	*c*
Fe(III)–μ_3–OMe	2.08–2.09	2.084(4)	2.04–2.11	2.06(3)	*c*	*c*	*c*	*c*
Fe(II)–μ_3–OMe	2.03–2.17	2.11(4)	2.09–2.17	2.13(3)	*c*	*c*	2.09–2.17	2.13(3)
Fe···Fe	3.02–3.30	3.18(9)	3.06–3.30	3.2(1)	3.20–3.25	3.23(2)	3.15–3.26	3.20(4)
ref	*d*		27		9f		27	

[a] Numbers in parentheses are estimated standard deviations. [b] **1** = $[Fe_{12}(O)_2(OMe)_{18}(OAc)_6(MeOH)_{4.67}]$, **3** = $[Fe_4(OMe)_5(MeOH)_3(OB)_4]$, **5** = $[Fe_6O(OMe)_{18}]^{2-}$, and **6** = $[Fe(OMe)(MeOH)(DPM)]_4$. [c] No examples present. [d] This work.

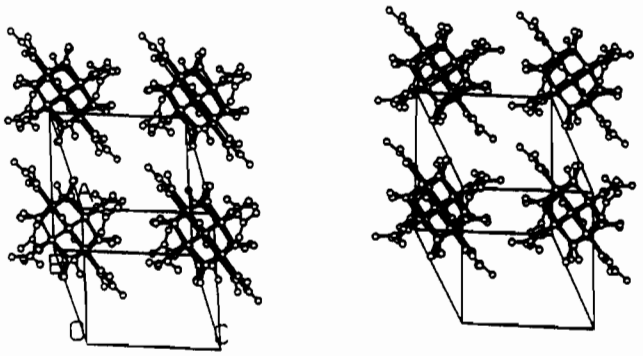

Figure 4. Crystal packing diagram of **1** depicting the second disorder model, which has one monodentate acetate and one methanol ligand.

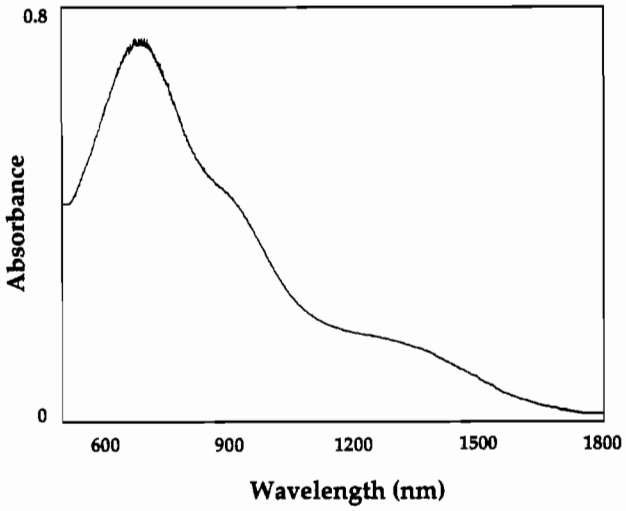

Figure 5. Electronic spectrum of **1** in 50% CD_2Cl_2/50% CD_3OD.

is that of Towe and Bradley, which has hexagonal close-packing of oxo, hydroxo, or water with iron(III) in the octahedral interstices.[8,36-38] Underpopulation of the iron(III) sites gives a crystallographic repeat unit of four oxygen layers, as opposed to the six found for the related iron oxide hematite (α-Fe_2O_3). We note, however, that other structural models have been proposed for ferrihydrite.[39] The structure of the Ft core is also complicated by the presence of phosphate, increasing amounts of which lower the crystallinity.[6] The hexagonal arrangement of oxygen atoms proposed for ferrihydrite differs from the cubic close-packing found for **1**, having an ABAB... repeat versus an ABCABC... repeat unit in the cubic case.[4b] In addition, **1** contains both iron(II) and iron(III), whereas, in Ft and ferrihydrite, the iron is completely oxidized. Despite these important differences, the structure of **1** does reproduce features of Ft and ferrihydrite, several of which have not been previously observed in a discrete, high-nuclearity iron complex. The μ_6-oxo ligands present in **1** are the fundamental structural element required for any close-packed arrangement of oxygen atoms, be it hexagonal or cubic. Iron atoms occupy octahedral positions in the oxygen atom lattice array of **1**, with the metal ions sharing octahedral coordination edges. Furthermore, the exclusive oxygen coordination for iron in **1** is like that found for the Ft and ferrihydrite. Single-layered structures are known for discrete polyiron oxo complexes,[10,11,14] but **1** is the only cluster thus far to have a three-dimensional lattice array of iron and oxygen atoms.

Vibrational and Electronic Spectroscopic Characterization. The IR spectrum of **1** offers some insights into the transformation that occurs upon drying crystals of the complex. Spectra taken before and after the process are almost the same, except for three minor differences. The broad OH stretching frequency shifts from 3450 to 3240 cm^{-1}, and two bands, located at 1262 and 802 cm^{-1}, disappear upon drying. These changes signal some structural rearrangement, the exact nature of which is unclear. The presence of an OH stretch in the dried powder of **1** indicates that some methanol is retained which, together with the measured weight loss and elemental analysis, suggests the formulation $[Fe_{12}(O)_2(OMe)_{18}(OAc)_6(MeOH)_2]$. Several of the IR spectral features can be assigned, including the ν_{as} and ν_s of the acetate ligands, which occur at 1560 and 1414 cm^{-1}, respectively. We tentatively attribute peaks at 1077 and 1025 cm^{-1} to C–O stretches of the methoxide bridges.

From solubility studies, it appears that some polymerization occurs during the transformation. The crystals of **1** are slightly soluble in THF and CH_2Cl_2, whereas the dried powder is only soluble in a mixture of methanol and a nonpolar solvent, such as CH_2Cl_2, and its electronic spectrum was therefore recorded using this mixture. Although the measured absorption features obey Beer's law, we have no other evidence that **1** remains intact upon dissolution.

The electronic absorption spectrum of **1** has an intense peak in the UV region below 300 nm, with a shoulder at 338 nm. We attribute this feature to a methoxide-to-iron charge transfer transition, and other iron(II) and iron(III) alkoxides exhibits similar absorption bands.[27,40] In addition, a broad absorption band occurs at 694 nm with shoulders at approximately 900 and 1250 nm, as shown in Figure 5. We assign these absorptions to iron(II) and iron(III) ligand field and intervalence charge transfer (IVCT) transitions, although it is difficult to assign specifically the individual components.[41,42] The electronic properties of the related mixed-valent cubane **3**, which contains the $\{Fe_4(OMe)_4\}^{5+}$ core, have been assigned, however, and a comparison of results for the two complexes is enlightening.[27] In **3**, a band at 690 nm

(36) Massover, W. H.; Cowley, J. M. *Proc. Natl. Acad. Sci. U.S.A.* **1973**, *70*, 3847.
(37) Towe, K. M. *J. Biol. Chem.* **1981**, *256*, 9377.
(38) Yang, J.; Takeyasu, K.; Somlyo, A. P.; Shao, Z. *Ultramicroscopy* **1992**, *45*, 199.
(39) (a) Eggleton, R. A.; Fitzpatrick, R. W. *Clays Clay Miner.* **1988**, *36*, 111. (b) Manceau, A.; Combes, J.-M.; Calas, G. *Clays Clay Miner.* **1990**, *38*, 331. (c) Eggleton, R. A.; Fitzpatrick, R. W. *Clays Clay Miner.* **1990**, *38*, 335.
(40) Snyder, B. S.; Patterson, G. S.; Abrahamson, A. J.; Holm, R. H. *J. Am. Chem. Soc.* **1989**, *111*, 5214.
(41) (a) Figgis, B. N. *Introduction to Ligand Fields*; Interscience Publishers: New York, 1966. (b) Lever, A. B. P. *Inorganic Electronic Spectroscopy*, 2nd ed.; Elsevier Publishing Co.: New York, 1984.
(42) (a) Allen, G. C.; Hush, N. S. *Prog. Inorg. Chem.* **1967**, *8*, 357. (b) Hush, N. S. *Prog. Inorg. Chem.* **1967**, *8*, 391.

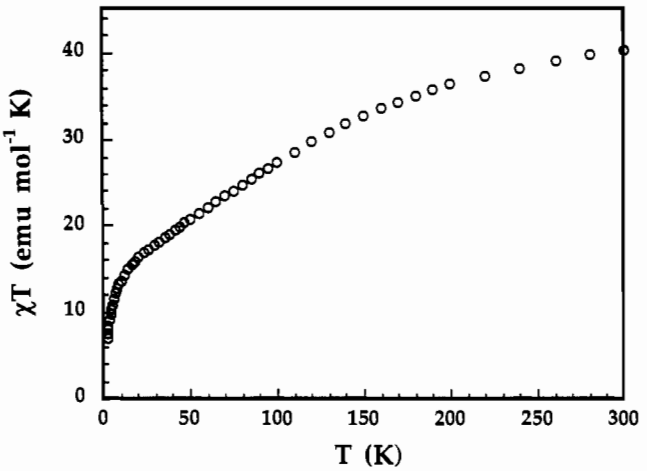

Figure 6. Plot of χT (emu mol^{-1} K) versus T (K) for a solid sample of **1**.

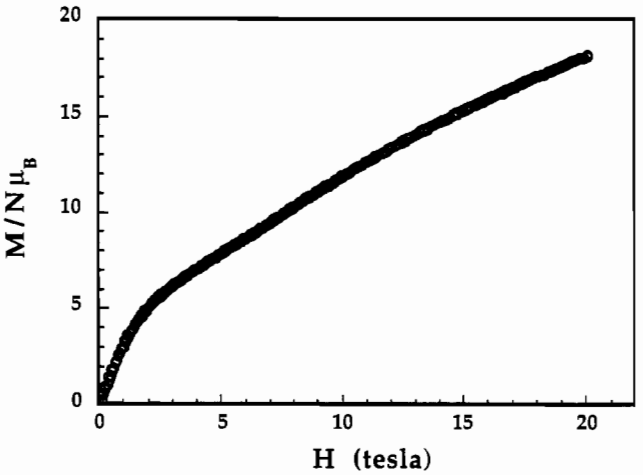

Figure 7. Magnetization of solid **1** from 0 to 20 T at 1.4 K.

was attributed to an iron(II) ligand field transition of $^5T_{2g} \rightarrow {}^5E_g$ parentage, and a second peak at 900 nm was assigned to an iron(II,III) IVCT transition. The corresponding features in **1** are located at 694 and 925 nm and are tentatively given the same assignments. The shoulder at 1250 nm in the spectrum of **1** is more difficult to assign, since no related feature was found for **3**. It could be another IVCT transition or a second component of the $^5T_{2g} \rightarrow {}^5E_g$ absorption. In the electronic spectrum of $[Fe(H_2O)_6]^{2+}$, the ligand field transition is split by a Jahn–Teller distortion into two peaks, occurring at 961 and 1204 nm.[41] The all-iron(II) cube **6** exhibits two bands at 809 and 1125 nm, which also were attributed to a lowering of the symmetry about the iron(II) ions.[27]

If the assignment of the optical bands for **1** is correct, the energy, E_{OP}, of the IVCT transition in both **1** and **3**, 10 800 and 11 000 cm^{-1}, respectively, is greater than that found for other mixed-valent iron complexes. Several diiron(II,III) compounds have $E_{OP} < 8000$ cm^{-1}.[40,43] On the other hand, examples from mineralogy, which contain edge-shared mixed-valent iron octahedra, have IVCT transitions with $E_{OP} > 12\,000$ cm^{-1}.[31] Partially oxidized vivianite, which has a diiron(II,III) core bridged by two hydroxide ligands, has the highest energy IVCT transition, 15 870 cm^{-1}, for this class of molecules. The structural study and electronic spectrum indicate that **1** is a class II mixed-valent complex in the Robin and Day scheme.[44] Variable-temperature Mössbauer studies discussed below support this conclusion.

Magnetic Properties. The variable-temperature magnetic susceptibility, χ, of a sample of **1**, dried under vacuum, was measured at 5 kG from 2.5 to 300 K, and a plot of the molar χT versus temperature is depicted in Figure 6. The complex exhibits overall antiferromagnetic behavior, with χT decreasing from 40.3 emu mol^{-1} K at 300 K to 7.04 emu mol^{-1} K at 2.5 K. The calculated χT for four iron(III) and eight iron(II) cations with no exchange coupling is 46.5 emu mol^{-1} K, assuming g values of 2.0 for iron(III) and 2.2 for iron(II).[22] As a result of exchange coupling between iron atoms, the net spin of the molecule, S_T, can adopt integral values from 0 to 26. In addition, the magnetic properties of iron(II) are strongly affected by zero-field splitting and orbital contributions.[45] Because of the large number of nearest-neighbor Fe···Fe interactions in **1**, a theoretical treatment was not possible, and we were unable to determine the ground-state spin of the molecule. For complexes **3** and **6**, both of which contain $\{Fe_4(OMe)_4\}^{n+}$ cubes like those present in **1**, the strength of the magnetic exchange interaction was determined to be $1 \leq |J| \leq 3$ cm^{-1} ($H = J\sum_i^j S_i \cdot S_j$ where $j > i$).[27] For tetrairon(II) cubane complex **6**, the coupling is ferromagnetic, whereas, for the mixed-valent cube **3**, the interaction is antiferromagnetic. The small magnitude of the coupling constants and their variability in sign suggest that the exchange interactions in **1**, which is composed of four fused iron–oxygen cubes, will be complex. In addition, spin frustration will almost certainly be present.[46]

A high-field, low-temperature magnetization study at 1.4 K was undertaken to determine whether **1** has a well-separated ground state in an applied field. As is evident from Figure 7, the field dependence of the magnetization did not follow the expected Brillouin function behavior characteristic of a single S_T value.[22] The magnetism did not saturate, and no remnant magnetism was observed at zero field after exposure to the field. The value attained at 20.0 T was 18.2 μ_B, which corresponds to a S_T between 8 and 9, assuming an average g value of 2.13 for the complex. The maximum possible value for four iron(III) and eight iron(II) atoms is 55. Because saturation was not observed, the lowest lying excited levels of the spin manifold of **1** appear to be close in energy to the ground state. Zero-field splitting within each spin multiplet further contributes to the complexity of the observed magnetism. The mixed-valent iron–methoxide cube **3** also did not saturate in an applied field.[27] By contrast, the ferromagnetically-coupled $\{Fe_4(OMe)_4\}^{4+}$ core of **6** saturated at a value consistent with a $S_T = 8$ ground state with appreciable anisotropy.[27]

Polynuclear iron oxo complexes exhibit a variety of magnetic phenomena, including spin frustration.[9-13,46] Overall antiferromagnetic behavior like that found for **1** has been observed for several other molecules, and for these cases, the magnetization does not saturate in large applied fields.[11-13] The inorganic core of Ft is antiferromagnetically exchange-coupled as well; however, uncompensated spin produces a bulk ferrimagnet.[47] A large density of states has been calculated for these polymetallic complexes, with the spin manifold approaching that of a bandlike structure.[10,48,49] A similar situation is realized in **1**.

Mössbauer Spectroscopy. Three different powdered samples of **1** were examined over a range of temperatures. Sample A,

(43) (a) Borovik, A. S.; Murch, B. P.; Que, L., Jr.; Papaefthymiou, V.; Münck, E. *J. Am. Chem. Soc.* **1987**, *109*, 7190. (b) Suzuki, M.; Oshio, H.; Uehara, A.; Endo, K.; Yanaga, M.; Kida, S.; Saito, K. *Bull. Chem. Soc. Jpn.* **1988**, *61*, 3907. (c) Borovik, A. S.; Papaefthymiou, V.; Taylor, L. F.; Anderson, O. P.; Que, L., Jr. *J. Am. Chem. Soc.* **1989**, *111*, 6183. (d) Mashuta, M. S.; Webb, R. J.; McCusker, J. K.; Schmitt, E. A.; Oberhausen, K. J.; Richardson, J. F.; Buchanan, R. M.; Hendrickson, D. N. *J. Am. Chem. Soc.* **1992**, *114*, 3815.

(44) Robin, M. B.; Day, P. *Adv. Inorg. Chem. Radiochem.* **1967**, *10*, 247.

(45) (a) Gerloch, M. *Magnetism and Ligand Field Analysis*; Cambridge University Press: Cambridge, U.K., 1983. (b) Gerloch, M. *J. Chem. Soc. A* **1971**, 2307.

(46) Delfs, C. D.; Gatteschi, D.; Pardi, L. *Comments Inorg. Chem.* **1993**, *15*, 27.

(47) (a) Blaise, A.; Chappert, J.; Girardet, J. *C. R. Acad. Sci.* **1965**, *261*, 2310. (b) Mohie-Eldin, M.-E. Y.; Frankel, R. B.; Gunther, L. Manuscript in preparation.

(48) A recent overview is provided in: Gatteschi, D.; Pardi, L.; Sessoli, R. *Mater. Sci.* **1991**, *17*, 7.

(49) Several high-nuclearity iron–sulfur and –selenium clusters have been prepared and characterized: (a) You, J.-F.; Snyder, B. S.; Papaefthymiou, G. C.; Holm, R. H. *J. Am. Chem. Soc.* **1990**, *112*, 1067. (b) You, J.-F.; Papaefthymiou, G. C.; Holm, R. H. *J. Am. Chem. Soc.* **1992**, *114*, 2697.

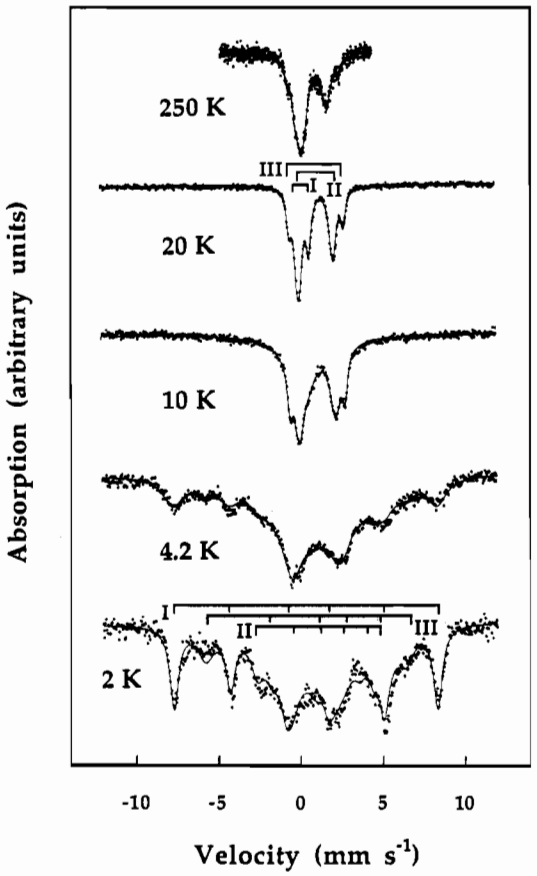

Figure 8. Mössbauer spectra of solid **1**, sample A, at 250, 20, 10, 4.2, and 2 K.

described previously,[15] was kept under nitrogen for several days prior to the experiment, whereas samples B and C were dried under vacuum for several hours. Mössbauer spectra of sample A are shown in Figure 8, and the corresponding spectra for sample B are available in the supplementary material. The temperature-dependent Mössbauer spectra of the three samples were identical except that sample A produced sharper lines, resulting in better resolved subcomponents.

Above 20 K, the Mössbauer spectra of samples A and B contain three distinguishable quadrupolar split resonances. A superposition of quadrupole doublets with Lorentzian line shapes was used to fit these spectra, the parameters of which are listed in Table 6 along with those for several other polynuclear iron–oxygen species. The composite fits are drawn as solid lines through the data points in both figures. Although **1** contains six crystallographically-unique iron sites, a three-site fit was sufficient to reproduce the experimental data. The isomer shift and quadrupole splitting of component I in both samples is consistent with high-spin iron(III). The ferric spectral parameters for **1**, $[Fe_{11}O_6(OH)_6(OBz)_{15}]$ (**8**), $[Fe_{16}MnO_{10}(OH)_{10}(OBz)_{20}]$ (**9**), and the iron(III) component of **3** are all quite similar. Spectral subcomponents II and III for **1** have Mössbauer spectral parameters characteristic of iron(II), with almost identical isomer shifts, 1.28 and 1.29 mm s^{-1}, respectively. Their quadrupole splittings values, however, are quite different, 2.02 versus 3.29 mm s^{-1}. A range of quadrupole splitting parameters is found for ferrous ion, two examples being the $\{Fe_4(OMe)_4\}^{n+}$ cube complexes **3** and **6** (Table 6). The spectral parameters determined for the two samples A and B are quite similar, the major difference being the width at half-height, Γ, for the spectral features.

Assuming that the recoil-free fractions are identical for all the iron sites, the integrated absorption for the three spectral components of **1** will reflect the relative proportions of iron(II) and iron(III).[50] The predicted proportions of Fe(II) and Fe(III) from the structural study are 67 and 33%, respectively. The measured Fe(II) and Fe(III) values at 20 K are 71 and 29% for sample A and 70 and 30% for sample B, respectively. Subcomponent II of the ferrous subsites accounts for approximately 55% of the total absorption area, or six iron(II) ions, and subcomponent III arises from the two remaining iron(II) sites. These values are quite close to the predicted percentages; the small discrepancies probably result from different recoilless fractions for the ferrous and ferric subsites in the cluster. The differences in recoil free fractions are accentuated at higher temperatures, leading to the larger discrepancy in the experimental ratios for the two oxidation states at 250 K.

The Mössbauer parameters for several different forms of Ft and ferrihydrite are also presented in Table 6. As for the model complex **1**, the mixed-valent derivatives have well-resolved resonances for the iron(II) and iron(III) components. The iron(III) spectral parameters for the different Ft cores and ferrihydrite[51] are quite similar to those of **1**, but there are differences in the iron(II) parameters.[52-60] Mössbauer spectral data have been obtained for ferrous components in Ft generated under a variety of conditions, as indicated in Table 6. The Mössbauer resonances for all these iron(II) examples have quadrupole splittings approaching 3.0 mm s^{-1}, as does component III of **1**. In contrast, the major iron(II) component of **1** has $\Delta E_Q = 2.02$ mm s^{-1}, a value that has not been observed in any Ft core sample to the best of our knowledge. Babingtonite has one ferrous component with a quadrupole splitting of 2.41 mm s^{-1},[31] and phosphate–iron(II) interactions appear to lower ΔE_Q slightly.[58]

The temperature dependence of the Mössbauer spectra of **1** has been investigated from room temperature down to 2 K. The 250 K spectra for all three samples of **1** reveal that no electronic delocalization occurs at this temperature on the Mössbauer time scale. This result is consistent with the behavior of the mixed-valent iron–oxygen cube **3**[27] and mixed-valent forms of Ft proteins. In contrast, a number of diiron(II,III) complexes with oxygen bridging ligands exhibit valence delocalization on the Mössbauer time scale.[43,61]

Below 20 K, the spectra of all three samples exhibit the onset of intermediate spin relaxation phenomena. At the lowest temperature studied, 2 K, sharp magnetic features at the outer edges of the spectrum are superimposed on a broad absorption area at the center. With increasing temperature, these magnetic subcomponents diminish in intensity and the broad central absorption area narrows, eventually collapsing to the three quadrupolar sites discussed above. The data were fit by a least-squares procedure to a set of three overlapping magnetic subsites. The large unresolved central absorption areas in the 2 and 4.2 K spectra were simulated by including a broad background envelope and a broad quadrupolar resonance, and these two spectral features account for the absorption area not attributed to sites I–III. Satisfactory fits for the three different samples were obtained by using the same Mössbauer spectral parameters with the chief difference being the magnitude of the line widths.

(50) Greenwood, N. N.; Gibb, F. C. *Mössbauer Spectroscopy*; Chapman & Hall, Ltd.: London, 1971.
(51) Murad, E.; Bowen, L. H.; Long, G. J.; Quin, T. G. *Clay Miner.* **1988**, *23*, 161.
(52) Watt, G. D.; Frankel, R. B.; Papaefthymiou, G. C. *Proc. Natl. Acad. Sci. U.S.A.* **1985**, *82*, 3640.
(53) St. Pierre, T. G.; Bell, S. H.; Dickson, D. P. E.; Mann, S.; Webb, J.; Moore, G. R.; Williams, R. J. P. *Biochim. Biophys. Acta* **1986**, *870*, 127.
(54) Rohrer, J. S.; Joo, M.-S.; Dartyge, E.; Sayers, D. E.; Fontaine, A.; Theil, E. C. *J. Biol. Chem.* **1987**, *262*, 13385.
(55) Jacobs, D.; Watt, G. D.; Frankel, R. B.; Papaefthymiou, G. C. *Biochemistry* **1989**, *28*, 9216.
(56) Bauminger, E. R.; Harrison, P. M.; Nowik, I.; Treffry, A. *Biochemistry* **1989**, *28*, 5486.
(57) Bauminger, E. R.; Harrison, P. M.; Hechel, D.; Nowik, I.; Treffry, A. *Biochim. Biophys. Acta* **1991**, *1118*, 48.
(58) Cheng, Y. G.; Chasteen, N. D. *Biochemistry* **1991**, *30*, 2947.
(59) Watt, G. D.; Frankel, R. B.; Jacobs, D.; Huang, H.; Papaefthymiou, G. C. *Biochemistry* **1992**, *31*, 5672.
(60) Mielczarek, E. V.; Andrews, S. C.; Bauminger, E. R. *BioMetals* **1992**, *5*, 87.
(61) Surerus, K. K.; Münck, E.; Snyder, B. S.; Holm, R. H. *J. Am. Chem. Soc.* **1989**, *111*, 5501.

Table 6. Selected Mössbauer Spectral Parameters for Polynuclear Iron–Oxygen Species[a]

compound	T, K	δ, mm s^{-1}	ΔE_Q, mm s^{-1}	Γ, mm s^{-1}	A, %	H_{hf}, T	ref
1, sample A[b]	250	0.36	0.48	0.58	35		*c*
		1.18	1.54	0.74	60		
		1.18	3.13	0.23	5		
	20	0.47	0.74	0.38	29		
		1.28	2.02	0.52	55		
		1.29	3.29	0.34	16		
	2	0.47	–0.08[d]	0.66	30[e]	49.7	
		1.2	–0.64	0.80	13	22	
		1.2	–1.41	0.80	18	38	
1, sample B	250	0.42	0.47	0.63	42		*c*
		1.17	1.40	0.67	50		
		1.18	3.05	0.30	8		
	20	0.47	0.80	0.46	30		
		1.19	2.13	0.55	54		
		1.22	3.26	0.35	16		
	2	0.47	–0.08[d]	0.90	27[e]	49.7	
		1.2	–0.64	1.0	14	22	
		1.2	–1.41	1.0	12	38	
$[Fe_{11}O_6(OH)_6(OBz)_{15}]$ (**8**)	80	0.50	0.91		100		12
$[Fe_{16}MnO_{10}(OH)_{10}(OBz)_{20}]$ (**9**)[f]	80	0.51	0.77		100		13
$[Fe_4(OMe)_5(MeOH)_3(OBz)_4]$ (**3**)	180	0.47	0.87	0.34	26		27
		1.24	2.97	0.38	74		
$[Fe(OMe)(MeOH)(DPM)]_4$ (**6**)	80	1.24	2.25	0.40	100		27
human spleen Ft[g]	78	0.47	0.69		100	49.4	53
horse spleen Ft	100	0.45	0.72		100		52
reconst Ft/phosphate	77	0.50	0.68		100		58
Fe(II) + Apo Ft	80	1.26	3.10		100		55
electrochemically reduced holo Ft[h]	100	0.47	0.63		31		52
		1.28	2.82		69		
Fe(II) + holo Ft	80	0.50	0.71		66	49.7	55
		1.34	3.04		34		
partially reconst Ft[i]	90	0.49	0.70	0.44	64		57
		1.34	2.94	0.42	14		
		1.38	3.33	0.32	22		
partially reconst Ft/phosphate[i]	77	0.37	0.94		75		58
		1.55	2.61		25		
ferrihydrite[j]	300	0.35	0.90	0.42	56	48.6	51
		0.35	0.55	0.31	44		

[a] δ = isomer shift; ΔE_Q = quadrupole splitting; Γ = width at half peak height; A = resonant absorption area normalized to 100% for the total resonant area; H_{hf} = magnetic hyperfine field. [b] The samples A and B of **1** are described in the text. [c] This work. [d] For magnetically-split spectra, $\epsilon = (1/4)\Delta E_Q(3\cos^2\theta - 1)$. [e] A broad background absorption envelope and quadrupolar resonance at the center of the spectrum account for the remainder of the absorption area. See the text for a discussion of the fitting procedures. [f] See also ref 65. [g] All Ft samples were from horse spleen, unless otherwise noted. [h] The H_{hf} was reported to be the same as for fully oxidized Ft. [i] Many different examples are reported in the designated references. [j] The ferrihydrite sample studied was highly crystalline. Although a single-site fit was possible, a two-site fit gave an appreciably better result.

As shown in Table 6, the magnetic structure of site I, with a hyperfine field H_{hf} of 49.7 T, is characteristic of high-spin iron(III), and those of sites II and III, which have respective H_{hf} values of 22 and 38 T and large quadrupolar perturbation parameters, are typical of high-spin iron(II). For the ferrous ions, orbital and dipolar contributions to the magnetic hyperfine field diminish the field produced by the Fermi contact interaction.[50] The much reduced hyperfine fields of the ferrous sites as compared to the iron(III) subcomponent produce proportionally lower nuclear spin Larmor precession frequencies. Thus, intermediate spin-relaxation spectral broadening is observed for the iron(II) features down to 2 K, whereas the iron(III) site has completely crossed into the slow relaxation regime at this temperature.

The main interactions responsible for the slow spin relaxation in **1** in the absence of an applied field are difficult to establish unequivocally from powder samples. Such magnetic hyperfine interactions may originate from either molecular anisotropy or collective magnetic interactions within **1** itself, which produce particle-like superparamagnetism.[62] Substantial molecular anisotropy has resulted in slow paramagnetic relaxation in both Kramers[61] and non-Kramers systems,[63] **1** being an example of the latter. Related relaxation phenomena in ac susceptibility measurements for a dodecanuclear manganese complex were also recently reported.[64] The properties of the lower lying spin states of **1**, however, could not be determined from the powder magnetic studies, so that magnitude of the molecular anisotropy is unknown. Both experiment and theory indicate that the onset of behavior typical for extended solids, including collective magnetic interactions, appears to occur in the vicinity of 10 metal ions for discrete molecular clusters.[65] Superparamagnetic-like behavior may result from the extremely small domain size of such species.[46] The temperature dependence of the Mössbauer spectral features of **1** at low temperatures is consistent with this phenomenon. Magnetic hyperfine structures observed in the absence of an applied magnetic field for **8** and **9** have been attributed to this relaxation effect.[65] Furthermore, superferromagnetic interactions between ferrihydrite particles were recently invoked to explain in detail Mössbauer relaxation spectra, and such interactions may also be operative in **1**.[66] Because the cluster contains 12 metal ions and its Mössbauer properties are consistent with superparamagnetic-like behavior, we favor this explanation for the slow spin relaxation.

Implications for Biomineralization in Ferritin. Iron deposition in Ft occurs by two different processes which are distinguished

(62) Morrish, A. H. *The Physical Principles of Magnetism*; John Wiley & Sons: New York, 1965.
(63) Surerus, K. K.; Hendrich, M. P.; Christie, P. D.; Rottgardt, D.; Orme-Johnson, W. H.; Münck, E. *J. Am. Chem. Soc.* **1992**, *114*, 8579.
(64) (a) Sessoli, R.; Tsai, H.-L.; Schake, A. R.; Wang, S.; Vincent, J. B.; Folting, K.; Gatteschi, D.; Christou, G.; Hendrickson, D. N. *J. Am. Chem. Soc.* **1993**, *115*, 1804. (b) Sessoli, R.; Gatteschi, D.; Caneschi, A.; Novak, M. A. *Nature* **1993**, *365*, 141.
(65) Papaefthymiou, G. C. *Phys. Rev. B* **1992**, *46*, 10366 and references therein.
(66) Cianchi, L.; Mancini, M.; Spina, G.; Tang, H. *J. Phys.: Condens. Matter* **1992**, *4*, 2073.

by the site of iron(II) oxidation.[6,67] In one, the protein sheath itself conveys ferroxidase activity,[68] and in the other, oxidation occurs directly on the iron mineral core in a heterogeneous reaction. Although both the former, catalytic, and latter, autoxidation, mechanisms operate simultaneously, one generally predominates, depending on reaction conditions.[69,70]

Ferroxidase activity has long been known for wild type mammalian Ft,[68] and a specific catalytic site has been located on the human liver Ft H chain by site-directed mutagenesis and crystallographic studies.[7,71] By contrast, no ferroxidase activity has been observed for the L chain of mammalian Ft, and recombinant Ft composed of all H or all L subunits exhibits vastly different iron(II) oxidation rates.[70,72,74] For Ft with all L subunits, autoxidation predominates, regardless of the deposition conditions. Naturally-occurring mammalian Ft has a mixture of the two subunit chains 4 and 16% H for human liver Ft and horse spleen Ft, respectively, and these natural forms exhibit a slightly diminished ferroxidase activity as compared to recombinant H-chain Ft, but one that is still significantly faster than that for apoFt composed of peptide subunits which do not have a protein catalytic site.

The mixed-valent iron complex **1** may provide some insight into the heterogeneous autoxidation reaction in Ft. The two (μ_6-oxo)diiron(III) centers can be considered as a nucleus of the iron–oxo–hydroxo core, with iron(II) bound to its surface through bridging oxygen ligands. During autoxidation, iron(II) most likely coordinates to surface oxygen atoms prior to the redox step. Coordination of negatively charged hydroxide, oxide, or phosphate ligands to $[Fe(H_2O)_6]^{2+}$ would facilitate the oxidation reaction by lowering the reduction potential. Subsequent deprotonation of water coordination to iron(III) formed in this step would extend the ferrihydrite core. For naturally occurring and recombinant H-chain Ft, a mixed-valence complex of the size of **1** would probably not be present at any point during cluster growth, because the ferroxidase center provides mononuclear ferric ions in abundance for core growth. For recombinant L-chain Ft or other forms of the protein lacking ferroxidase activity, however, complex **1**, or, more accurately, **1** with hydroxide in place of the methoxide ligands, may represent a stage in core growth. Autoxidation on the mineral surface is the most likely means of core deposition, and mixed-valent iron species are possible intermediates in this process. In support of this hypothesis, both iron(II) and iron(III) have been observed in Mössbauer studies of Ft biomineralization. A ferrous subcomponent with $\Delta E_Q \sim 2.0$ mm s^{-1}, like that found for **1**, has not yet been observed in these investigations, however.[52,54-60] Several iron(III) clusters have been reported by others,[56,75] and one mixed-valent diiron(II,III) species has been observed by EPR spectroscopy.[76]

Acknowledgment. This work was supported by grants from the National Science Foundation and the Office of Naval Research. The Francis Bitter National Magnet Laboratory was supported by the National Science Foundation. K.L.T. is grateful to the National Science Foundation for a Graduate Research Fellowship. We thank E. J. McNiff, Jr., of the Francis Bitter National Magnet Laboratory for carrying out the magnetization measurement of **1**. Dr. A. Caneschi is gratefully acknowledged for experimental advice and assistance.

Supplementary Material Available: A table of atomic thermal parameters for **1**, a complete listing of bond distances and angles for **1**, and variable-temperature Mössbauer spectra of sample B of **1** (7 pages). Ordering information is given on any current masthead page.

(67) (a) Macara, I. G.; Hoy, T. G.; Harrison, P. M. *Biochem. J.* **1972**, *126*, 151. (b) Macara, I. G.; Hoy, T. G.; Harrison, P. M. *Biochem. J.* **1973**, *135*, 785.
(68) Bryce, C. F. A.; Crichton, R. R. *Biochem. J.* **1973**, *133*, 301.
(69) Xu, B.; Chasteen, N. D. *J. Biol. Chem.* **1991**, *266*, 19965.
(70) (a) Sun, S.; Chasteen, N. D. *J. Biol. Chem.* **1992**, *267*, 25160. (b) Sun, S.; Arosio, P.; Levi, S.; Chasteen, N. D. *Biochemistry*, in press.
(71) Lawson, D. M.; Treffry, A.; Artymiuk, P. J.; Harrison, P. M.; Yewdall, S. J.; Luzzago, A.; Cesareni, G.; Levi, S.; Arosio, P. *FEBS Lett.* **1989**, *254*, 207.
(72) Levi, S.; Salfeld, J.; Franceschinelli, F.; Cozzi, A.; Dorner, M. H.; Arosio, P. *Biochemistry* **1989**, *28*, 5179.
(73) Wade, V. J.; Levi, S.; Arosio, P.; Treffry, A.; Harrison, P. M.; Mann, S. *J. Mol. Biol.* **1991**, *221*, 1443.
(74) Levi, S.; Yewdall, S. J.; Harrison, P. M.; Santambrogio, P.; Cozzi, A.; Rovida, E.; Albertini, A.; Arosio, P. *Biochem. J.* **1992**, *288*, 591.
(75) Yang, C.; Meagher, A.; Huynh, B. H.; Sayers, D. E.; Theil, E. C. *Biochemistry* **1987**, *26*, 497.
(76) Hanna, P. M.; Chen, Y.; Chasteen, N. D. *J. Biol. Chem.* **1991**, *266*, 886.